Photonic integrated circuits for millimeter-wave wireless communications

Microwave Photonic Integrated Circuits for Millimeter-Wave Wireless Communications

G. Carpintero, K. Balakier, Z. Yang, R. C. Guzmán, A. Corradi, A. Jimenez, G. Kervella, M. J. Fice, M. Lamponi, M. Chitoui, F. van Dijk, C. C. Renaud, A. Wonfor, E. A. J. M. Bente, R. V. Penty, I. H White, and A. J. Seeds

***Abstract*—This paper describes the advantages that the introduction of photonic integration technologies can bring to the development of photonic-enabled wireless communications systems operating in the millimeter wave frequency range. We present two approaches for the development of dual wavelength sources for heterodyne-based millimeter wave generation realized using active/passive photonic integration technology. One approach integrates monolithically two distributed feedback semiconductor lasers along with semiconductor optical amplifiers, wavelength combiners, electro-optic modulators and broad bandwidth photodiodes. The other uses a generic photonic integration platform, developing narrow linewidth dual wavelength lasers based on arrayed waveguide gratings. Moreover, data transmission over a wireless link at a carrier wave frequency above 100 GHz is presented, in which the two lasers are free-running, and the modulation is directly applied to the single photonic chip without the requirement of any additional component.**

***Index Terms*—Broadband communication, microwave photonics, millimeter wave communication, millimeter wave integrated circuits, photonic integrated circuits, semiconductor lasers.**

I. Introduction

PHOTONIC techniques have become key enablers to unlock future broadband wireless communications with multigigabit data rates in order to support the current trends of mobile data traffic, which is expected to increase 13-fold between 2012 and 2017 [1]. It is estimated that complex modulation formats making more efficient use of the spectrum will not suffice, and moving to carrier frequencies into the millimeter wave frequency range (30 to 300 GHz) will be necessary [2]. Several demonstrations have already been presented in the millimeter/sub-millimeter wavelengths, using different approaches to generate the carrier waves [3].

Within the all-electronics based approach, compound semiconductor technology has been considered the strongest for high-frequency applications. Integrated transmitter modules based on InP high-electron mobility transistor millimeter-wave (MMW) monolithic integrated circuits chipsets were used in the most successful demonstration of a wireless link at 120 GHz, transmitting HD video signals over 1-km distance at 10 Gbps data rate [4]. Wireless link front ends with data rates up to 25 Gbps at a carrier frequency of 220 GHz have also been demonstrated using On-Off Keying (OOK) and complex 256-quadrature amplitude modulation [5].

Photonic techniques are an alternative approach having some inherent key advantages such as being broadly tunable, having an ultra-wide bandwidth and being able to be seamlessly connected to wired (fiber optic) networks. The two key components for realizing photonics-based continuous-wave generation of millimeter waves are optical signal sources together with optical-to-electrical (O/E) converters [6]. There are multiple optical signal generation techniques, the most promising of which is optical heterodyning. This method requires an optical signal source generating two different wavelengths that are mixed into a photodiode or photoconductor (used as photomixer). The generated signal is an electrical beat-note at a frequency given by the difference between the wavelengths. When the two wavelengths are generated from uncorrelated sources, the generated beat-note exhibits large phase noise fluctuations due to the linewidth of the lasers and to the relative wavelength fluctuation between them [7]. This prevents the use of complex codes, with negative impact on the maximum data rate.

Photonic-enabled wireless links have used different approaches to obtain suitable dual wavelength sources. Different MMW and TeraHertz (THz) photonic integrated sources have been demonstrated based on the monolithic integration of Distributed Feedback (DFB) lasers and light combining elements. Among the advantages brought by monolithic integration we can highlight the resulting compactness of the system and that the lasers will encounter the same environment fluctuations, thus reducing noise. The most common approach is to grow the two DFB lasers side by side. Using quantum-dash long cavities and combining the wavelengths using a Y-junction, tuning ranges from 2 to 20 GHz and optical linewidth around 1 MHz has been demonstrated [8]. A radically different structure is to place the two DFB lasers in-line, separated by a phase modulator [9]. The lower difference frequency becomes a critical parameter,

Manuscript received January 15, 2014; revised March 19, 2014; accepted February 20, 2014. Date of publication May 5, 2014; date of current version September 1, 2014. This work was supported by the European Commission and carried out within the framework of the European STREP project iPHOS (www.iphos-project.eu) under Grant 257539.

G. Carpintero, R. C. Guzmán, and A. Jimenez are with the Universidad Carlos III de Madrid,, 28911 Madrid, Spain (e-mail:guiller@ing.uc3m.es; rcguzman@ing.uc3m.es; ajgalind@pa.uc3m.es).

K. Balakier, M. J. Fice, C. C. Renaud, and A. J. Seeds are with the Department of Electronic and Electrical Engineering, University College London, London, WC1E 7JE, U.K. (e-mail:k.balakier@ucl.ac.uk; m.fice@ucl.ac.uk; c.renaud@ucl.ac.uk; a.seeds@ucl.ac.uk).

G. Kervella, M. Lamponi, M. Chitoui, and F. Van Dijk are with III–V Lab,, 91767 Palaiseau Cedex, France (e-mail:gael.kervella@3-5lab.fr; marco.lamponi@3-5lab.fr; mourad.chtioui@thalesgroup.com; frederic.vandijk@3-5lab.fr).

E. A. J. M. Bente and A. Corradi are with the COBRA Research Institute, Eindhoven University of Technology, 5612 AZ Eindhoven, The Netherlands (e-mail:e.a.j.m.bente@tue.nl; a.corradi@tue.nl).

Z. Yang, A. Wonfor, R. V. Penty, and I. H. White are with the Department of Engineering, University of Cambridge, Cambridge CB3 0FA, U.K. (e-mail: zy235@cam.ac.uk; aw300@cam.ac.uk; rvp11@cam.ac.uk; ihw3@cam.ac.uk).

Color versions of one or more of the figures in this paper are available online at http://ieeexplore.ieee.org

Digital Object Identifier 10.1109/JLT.2014.2321573

as the wavelength separation has to be larger than the combined widths of the stop bands of the two lasers so each one is transparent to the other.

Pushing the boundaries in millimeter wave wireless applications was the objective of the European Commission funded project iPHOS (Integrated photonic transceivers at sub-terahertz wave range for ultra-wideband wireless communications). This project established a crossroad between photonic-enabled millimeter-wave technologies and photonic integration efforts to support advanced wireless communications in the E-band (60–90 GHz) and F-band (90–140 GHz) [10], having already demonstrated a wireless link using two free-running monolithically integrated DFB lasers to generate a 146 GHz carrier, transmitting non-return-to-zero OOK at a data rate of 1 Gbps using external modulation [11].

This paper presents the two approaches that were pursued within the iPHOS project to develop a photonic integrated circuit (PIC) dual wavelength source for heterodyne-based millimeter wave generation. The two device structures are described in Section II. The characterization and performance of both devices, realized using two distinct active/passive integration technologies, is presented in Section III. Finally, Section IV describes a wireless link data transmission at a carrier wave frequency above 100 GHz, in which the two sources are free-running, and the modulation is directly applied to the chip without any additional discrete components being required.

II. Photonic Integrated Dual Wavelength Sources

We present two different approaches to the monolithic integration of a dual wavelength source for millimeter-wave frequency signal generation by optical heterodyning, each having a different set of advantages and disadvantages.

The first approach demonstrates for the first time a fully monolithic millimeter-wave wireless transmitter, including two DFB lasers and optical combiners for the dual wavelength generation, electro-optic modulators for data modulation, and, crucially, integrated high-speed photodiodes (PD) to generate the millimeter electrical signal. Semiconductor optical amplifiers (SOA) are also included to compensate the optical losses. This approach, which has the great advantage of continuous tuning of the wavelength spacing, requires a dedicated fabrication process flow to develop all these components in the same chip. Its main drawback is the relative broad linewidth of the optical modes (usually >300 kHz), limiting the purity of the signal [7].

The second approach aims to develop a dual wavelength source that can be fabricated on a Generic InP-based technology platform to access the cost reduction of a multi-project wafer run. This approach, limited by the building blocks available on the platform [12], developed a dual wavelength arrayed waveguide grating (AWG) laser structure. These were initially proposed for wavelength division multiplexed sources since they are able to deliver multiple wavelengths, with fixed frequency spacing, defined by the AWG (usually $\Delta\lambda \sim 100$ GHz). This is a limitation of the structure, as the wavelength spacing is not continuously tunable. As an advantage, a narrow channel bandwidth selection allows these devices to emit in a single mode despite the length of the cavity, producing very stable and reproducible devices [13]. Using such a structure, we have demonstrated the generation of a RF beat note at 95 GHz, with a -3 dB linewidth of 250 kHz, the narrowest RF linewidth generated from a free running dual wavelength semiconductor laser [14]. An important drawback of this device structure is that it employs cleaved facets to define the cavity, which severely limits its integration potential to add on-chip functionality. In the devices reported here, novel multimode interference (MMI) reflectors are used to avoid this limitation.

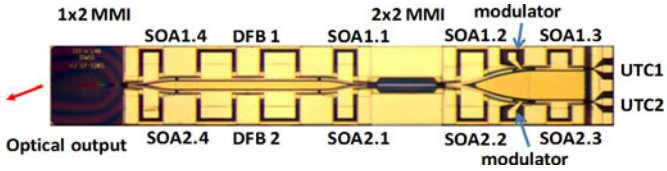

Fig. 1. Microscope view of the dual DFB dual wavelength source.

A. Dual Distributed Feedback Approach

The developed monolithic millimeter-wave wireless transmitter on a chip is presented in Fig. 1. As shown, it includes two DFB lasers of 1 mm length, both having a phase shift written in the middle of the Bragg grating to guarantee single mode operation. Their right-hand side outputs are combined in a 2×2 MMI coupler after passing through bent SOAs (SOA1.1 for the top laser, and SOA2.1 for the bottom). Both outputs of the MMI coupler, carrying the two wavelengths from each laser, are evanescently coupled to two monolithic Uni-Traveling Carrier photodiodes (UTC-PD) labeled UTC1 and UTC2 respectively. Between each MMI output and the UTC-PD, the light passes through another bent SOA (to boost the optical signal after passing through the combiner), an electro-optical modulator (to introduce the data modulation on-chip) and a straight SOA (to boost the signal entering the photodiode).

On the left-hand side of the chip, the light from the DFB lasers is combined in a 2×1 MMI coupler. This combiner is designed to allow phase noise reduction through optical injection locking. However, it also provides an optical access to the chip to monitor the optical spectrum. Some of the samples included in the fabrication batch included a phase section (PS) on one of the devices to allow tuning the beat note frequency through a fast wavelength tuning of one of the two wavelengths. The whole device is 4.4 mm long and 0.7 mm wide.

One of the main technological achievements of this approach has been the development of a fabrication process flow that allows the growth of the different components, in particular the high-speed photodiodes, in the single PIC. The layers were grown on a semi-insulating InP wafer in order to reduce the parasitic capacitance and get a sufficiently large detection bandwidth of the photodiodes. Active/passive integration is achieved using a butt-joint process. The active layers consist of 6 InGaAsP quantum wells. DFB lasers, SOAs and modulation sections contain the same quantum well stack. The Bragg grating is formed in an InGaAsP layer placed above the quantum wells and

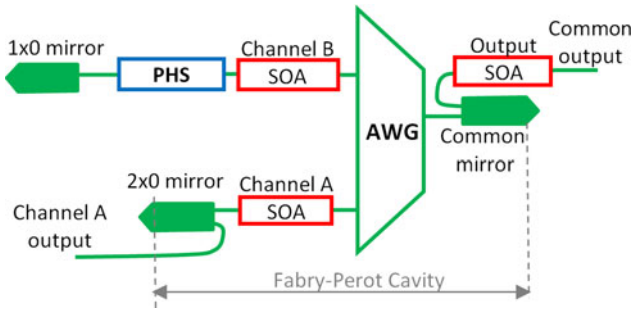

Fig. 2. Schematic of the AWG laser dual wavelength source showing the two types of channels. Type A, with SOA and Type B with SOA and PHS.

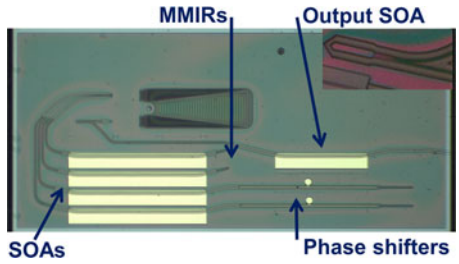

Fig. 3. Microscope view of the fabricated AWG laser dual wavelength source.

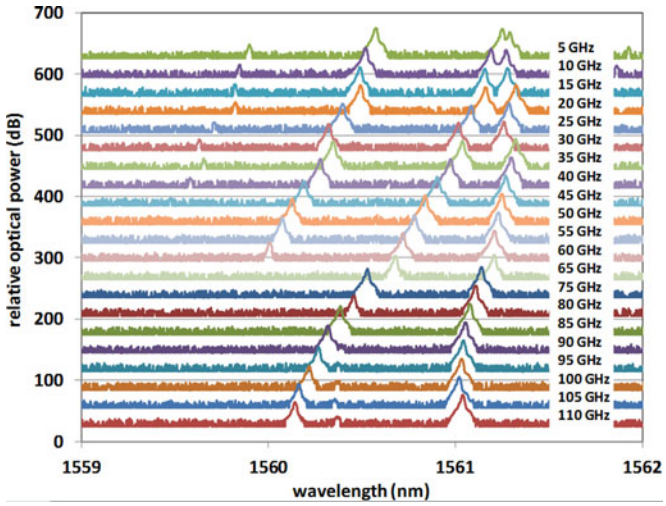

Fig. 4. Dual DFB optical spectra for different bias currents.

defined by e-beam lithography. The UTC layers are similar to the ones used in [15], are grown above the passive waveguide, to implement two 3×15 μm UTC-PD. The fabrication required 3 epitaxial growth steps. After wafer thinning and back metal deposition a first set of measurements were performed directly on the wafer. After these first measurements, chips were cleaved and mounted on AlN submounts.

B. Arrayed Waveguide Grating Approach

The alternative multi-wavelength structure that we present is based on an AWG laser using novel multimode interference reflectors (MIR) to define the mirrors [16], achieving a new fully monolithic structure. It is fabricated using active/passive integration on an InP technology multi-project wafer run, following the schematic in Fig. 2. The device has an extended cavity configuration built around the AWG, which acts as an intra-cavity filter. Since the cavity loss is minimal for a specific wavelength within each channel passband of the AWG, activating each channel SOA by current injection generates a specific wavelength. The common arm of the AWG multiplexes all the channel wavelengths on the common waveguide.

The novelty of the proposed device is that the AWG channel and common waveguides are terminated in MIR mirrors, using either a 2×0 mirror configuration when an optical output is desired (as shown for Channel type A in Fig. 2) or a 1×0 configuration to produce total reflection of the optical power (as shown for Channel type B). All AWG channels must include one SOA, to activate the corresponding channel wavelength. The two types of channels that we have defined in Fig. 2 differentiate whether it includes an Electro-Optic Phase Shifter (PHS) to allow wavelength tuning (channel type B) or it does not (channel type A). An output SOA, located at the common output of the chip, allows the optical output power from the chip to be boosted. The common waveguide routes the output power to an angled waveguide at an AR-coated facet to minimize back reflections.

Fig. 3 presents one realization of this photonic integrated circuit, produced within an InP technology multi-project wafer run. It shows a four channel AWG, with 1000-μm long SOAs at each channel. The AWG central wavelength is $\lambda o = 1550$ nm, the channel spacing $\Delta\lambda = 120$ GHz (0.96 nm) and the free spectral range (FSR) is 700 GHz ($\sim$ 6 nm). The two upper channels are type A, and the two bottom ones, type B, with 1000-μm long PHS each. All the channels are terminated with 1×0 MIR, to reduce the optical losses at the channels. The common arm of the AWG uses a 2×0 MIR to provide the multi-wavelength output, with 750-μm long output SOA. The total cavity length for type A channels is approximately 3.25 mm, 5 mm shorter than the AWG device presented in Ref. [16].

III. Device Characterization

A. Dual Distributed Feedback Devices

Using the left-hand side optical output of the device shown in Fig. 1, we have been able to measure simultaneously the spectrum of the optical signal generated by the chip and the generated high frequency electrical signal from the monolithically integrated UTC photodiodes when the DFB lasers were electrically tuned and some of the SOAs biased.

For the measurements showing the tuning range of the two wavelengths, one of the DFB lasers was biased with a current varying from 50 to 86 mA while the other was biased with a current varying within a 50 to 198 mA range. Within these bias ranges, the UTC photocurrent varied between 1.12 and 6.27 mA. During operation, the photodiode is reversed biased at 2.5 V. Dark current of $<$10 uA was measured at this bias point.

The measured optical spectra are presented in Fig. 4, where for the shown sample a continuous tuning of the optical frequency difference between the two DFB tones from 5 to

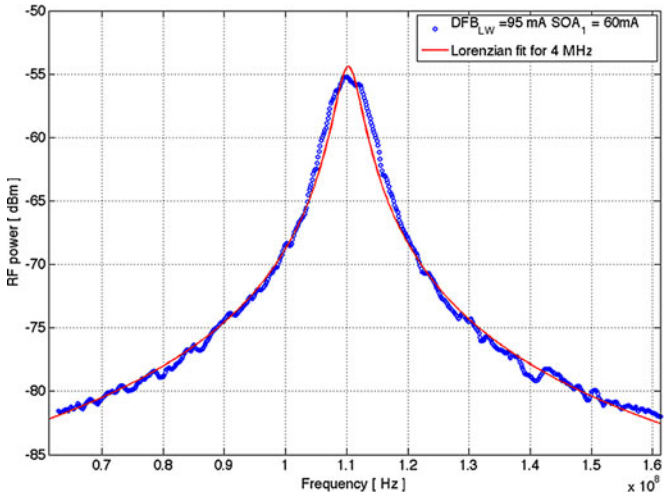

Fig. 5. Linewidth measurement of DFB laser (RBW = 2 MHz, VBW = 5 kHz).

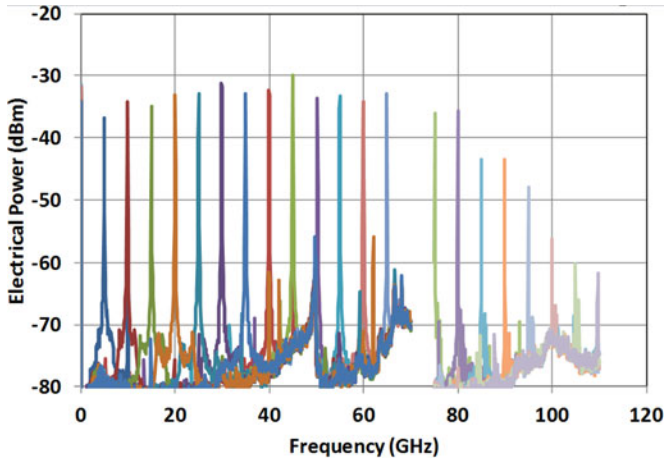

Fig. 6. Electrical spectra obtained for different laser biasing conditions.

110 GHz is observed. The wavelength tuning is thermal through changes in the DFB bias current. Also, as the two lasers are close to each other, we observe thermal cross-talk between the two lasers. For the upper curves on the graph (5–50 GHz), there is an additional optical tone. This is due to the tendency of each DFB lasers to have a dual mode behavior for higher bias currents. Indeed the DFB lasers, with an integrated phase shift, are single mode in the ideal case, where there are no reflections. In the integrated chip there are some residual reflections that can occur, for example, on the butt joints, in the MMI coupler or on the back of the photodiodes.

The linewidth of each laser was evaluated separately using the delayed self-heterodyne technique [17], with the result being presented in Fig. 5. Using a Lorentzian fit, the FWHM linewidth was assessed to be about 2 MHz for the DFB lasers with single-electrode and about 3 MHz for the DFB lasers which includes an additional, 100 um long passive PS for laser wavelength tuning.

The electrical spectra, shown in Fig. 6, were measured using a Rohde & Schwarz FSU67 electrical spectrum analyzer, with a FS-Z110 external mixer for measurements above 65 GHz.

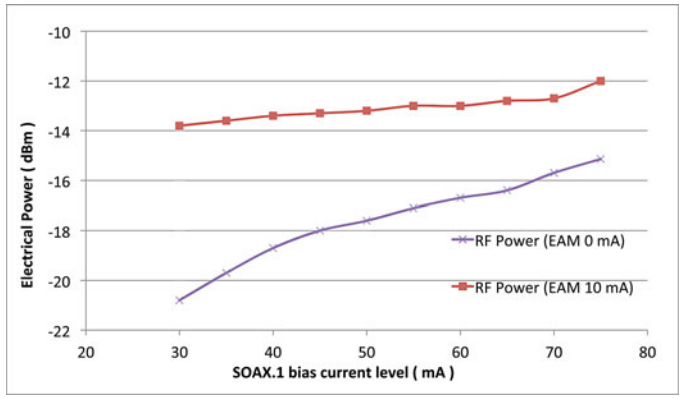

Fig. 7. Detected electrical power generated from the monolithically integrated photodiode when the modes are spaced 95,7 GHz at different bias levels of the modulator section.

Presence of the additional optical tone does not prevent the generation of the lower frequency range beat notes. Nevertheless, these additional optical mode lines may have a negative effect generating a photocurrent that is not useful for the purpose of signal generation and can potentially limit the maximum mm-wave power delivered. However, within the intended millimeter wave frequency ranges allocated to wireless in the E-band (71–76 and 81–86 GHz) the device is a dual mode source.

We were able to observe the beat note on the photodiode port over the full tuning range. In order to have a better idea of the bandwidth of the integrated photodiodes, we have corrected the power level of the detected high frequency tones by subtracting the losses of the cables and the probes and by normalizing it based on the measured photocurrent, estimating that the bandwidth of the photodiode is above 85 GHz. Further measurements on discrete devices cleaved from the wafers are needed in order to assess the bandwidth of these monolithic photodiodes.

The following test was done in order to determine the maximum electrical output power that could be generated at the integrated photodiode. The power emitted from the WR08 horn antenna at the RF probe was detected using an Agilent E4418B EPM series power meter with a W8486A power sensor with frequency range from 75 to 110 GHz. The two DFB lasers were biased at 95 mA, giving the generated beat note frequency 95.7 GHz. As shown on Fig. 7, by changing the current of the optical amplifiers at the output of each DFB (SOA1.1 and SOA2.1, which are connected to the same electrical contact on the submount), we demonstrate a maximum detected power of −12 dBm when the photodiode is reversed biased to −2.5 V with 8.76 mA generated photocurrent. The losses due to RF probe and signal free space propagation path (<3 cm) between antenna on the probe and power meter are not corrected.

B. *Arrayed Waveguide Grating Devices*

The AWG laser behavior can be assessed from both the channel and the common optical outputs. For this device, we have first measured the *L–I* characteristic at one of the outputs of a type B channel, with the phase shifter in open circuit. The optical spectrum is measured simultaneously on a Yokogawa

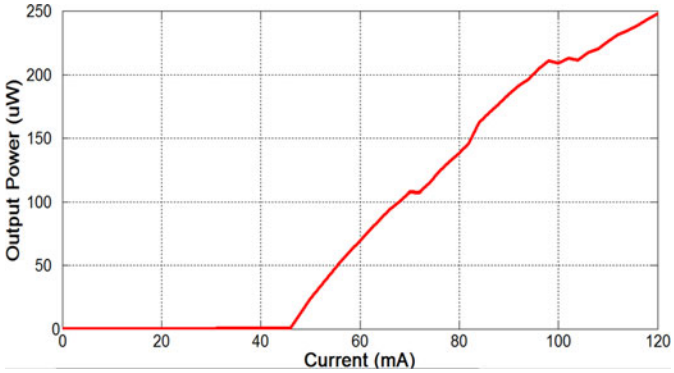

Fig. 8. *L–I* characteristic curve at the the channel output on a Type B channel. As the channel SOA is biased, the phase shifter remains in open circuit.

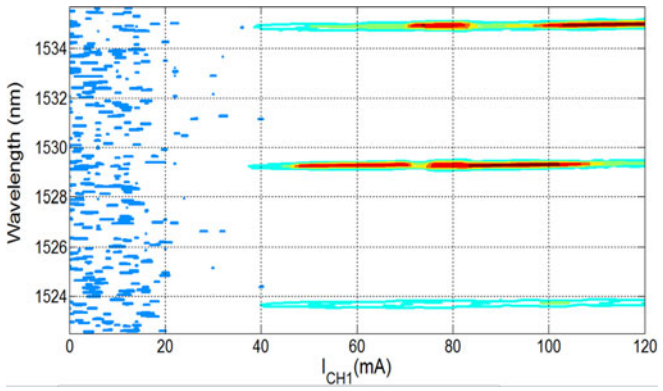

Fig. 9. Optical spectrum evolution at the channel output output on a Type B channel under the same conditions as Fig. 7.

AQ6370B Optical Spectrum Analyzer, splitting the optical signal to the optical power meter with a 90/10 splitter (90% to the power meter and 10% to the OSA).

The *L–I* trace as the channel SOA current increases is shown in Fig. 8 and the evolution of the corresponding optical spectrum on Fig. 9. For the *L–I* trace at the channel output, the EOPMs of both channels are kept disabled. The output optical power at 120 mA is about 250 μW and the threshold current value ($I_{\rm th}$) is about 44 mA. From the two figures, we conclude that the device emits in a single optical mode, and the kinks in the *L–I* trace correspond with jumps of the mode between adjacent FSR orders of the AWG. We have observed that the PHS can be used to control the FSR order in which the optical mode emits, rather than controlling a wavelength tuning mechanism, as the emission wavelength is strongly defined by the AWG channel. When the *L–I* characteristic is measured at the common output, we have to specify the current level for the Output SOA. The measured optical power for a channel SOA bias of 120 mA is 2 and 300 μW for Output SOA bias currents of 0 and 30 mA respectively. With an Output SOA current of 27 mA the losses produced by the AWG (measured on test structures to be above 20 dB) are compensated, and the same *L–I* trace is measured at the channel and common outputs. However, the most interesting feature is the dual wavelength regime. On the AWG structures having a boost SOA in the common channel, as the one in

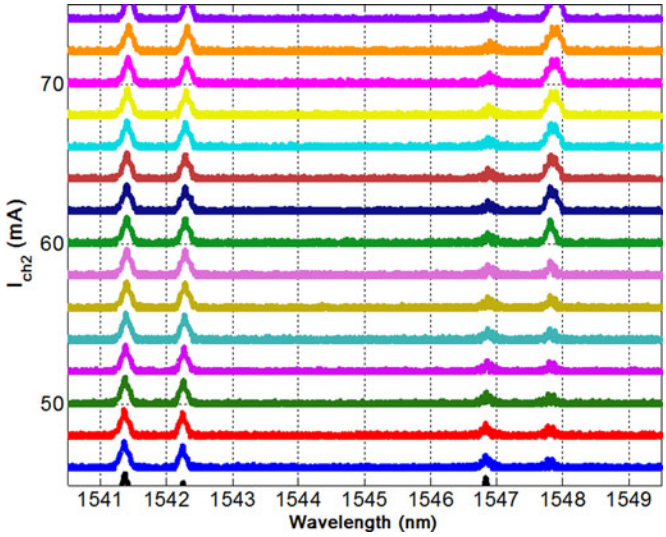

Fig. 10. Output optical spectrum mapping at the common output of the chip. Channel 1 is set a fixed bias current level of 80 mA whilst the channel 2 is swept from 44 mA to 74 mA with a Boost SOA bias current level of 10 mA.

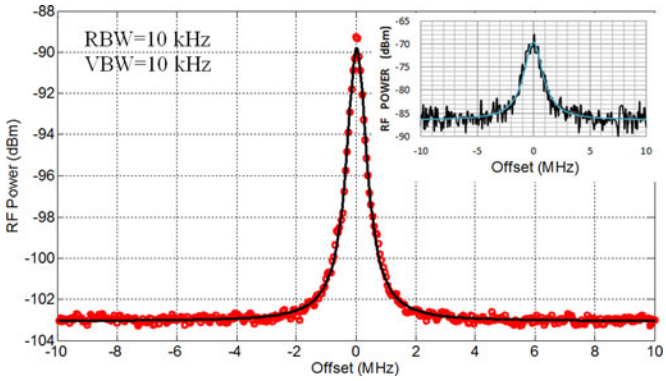

Fig. 11. Optical linewidth with channel SOA current at 50 mA and Boost SOA at 60 mA. The inset shows the 109 GHz beat note biasing the adjacent channel at 80 mA.

Reference [16], we have seen that the dual wavelength behavior regions are reduced due to mode competition of the two modes in this SOA.

To establish the dual-wavelength regions of the AWG laser with MMI reflectors, we have measured the optical output from the common output, when the channel SOA of two adjacent channels are biased. One channel is kept at a fixed current level above threshold (80 mA) while the other is swept from 44 mA (threshold level) to 100 mA in steps of 2 mA. The output SOA is also fixed at a constant bias level of 10 mA. As shown in Fig. 10, the device has a dual mode behavior over the entire current range. Above 70 mA, we find that lasing starts at a higher order of the AWG FSR. However as the frequency difference with this new FSR order is above 700 GHz, it would be suppress by the photodiode bandwidth. A delayed self-heterodyne measurement with Lorentzian fit to extract linewidth, shown in Fig. 11 reveals an optical linewidth below 100 kHz. The beat note spectrum measured using a fast photodiode (XPDV4120R) and FS-110

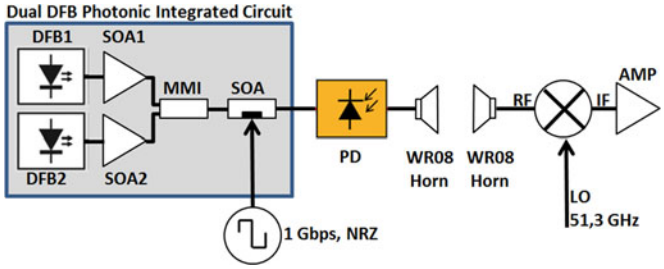

Fig. 12. Schematic of the constructed 105,4 GHz wireless link consisting of an optical mm-wave carrier generation using a dual DFB photonic integrated circuit with on chip data modulation.

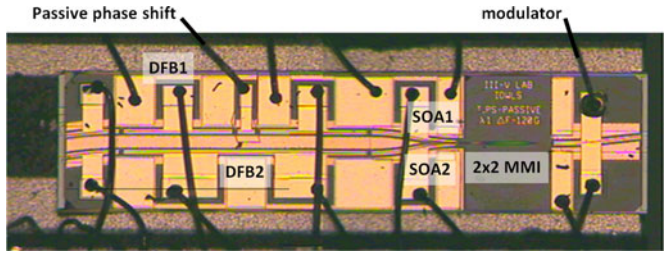

Fig. 13. Photograph of the dual DFB used for the wireless data transmission, represented by the dual DFB PIC box in the schematic of the wireless link.

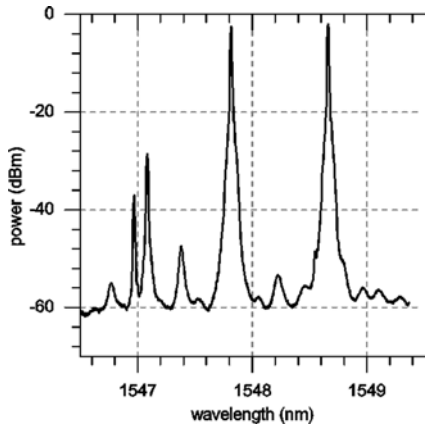

Fig. 14. Two tones separated by 0.85 nm produce a beat frequency within the F band.

external mixer is shown at the inset with the two central adjacent channel SOAs biased at 80 mA and 50 mA respectively, and the output SOA at 60 mA to increase the optical output power.

Although the emission wavelengths are fixed by the channel pass-bands of the AWG, this structure has been shown to produce optical modes with very narrow optical linewidth (<200 kHz) without any phase noise reduction scheme, separated at multiples of the channel spacing which enables them to generate signals within the THz region [18].

C. Comparison

We have shown that a dual wavelength source implemented by monolithic integration of two DFB has the great advantage of having a large tuning range, here demonstrated to cover the entire E-band range (60–90 GHz). The main concern is the linewidth of the optical modes. This is precisely the strong point for dual wavelength sources based on AWG lasers, exhibiting free running modes below 200 kHz. Due to the flexibility of the wavelength tuning, we have chosen the dual DFB devices to build a wireless data transmission experiment. In addition, this decision was based on the fact that the used device included a short SOA section at the angled facet to allow high-speed on-chip data modulation. It is worth highlighting that any on-chip modulator scheme (short SOA, EAM, Mach-Zehnder) that is external to the laser resonator can now be implemented to any of the presented designs, as both are fully monolithic structures that do not require the chip facets to establish the laser.

IV. Wireless Link

The millimeter wave wireless data transmission experimental setup is shown in Fig. 12. The sample, shown in Fig. 13, was processed in the same batch as the sample presented in section II. It includes two 1 mm-long DFB lasers, one of which has an integrated passive phase shift section in the middle of the Bragg grating for wavelength tuning. The outputs of the two lasers are combined, after passing through SOAs, on a 2 × 1 MMI coupler, and then pass through an SOA (used as a modulator) before the waveguide outputs the light at the chip facet with an angled termination to minimize reflections.

The device is operated by biasing DFB1 at 95 mA, DFB2 at 240 mA, SOA1 at 51 mA, SOA2 at 40 mA and Mod at 60 mA. This produces two wavelengths at the output, as shown in Fig. 14, separated by 0.85 nm (which corresponds to an RF frequency of 105.4 GHz). The power difference between the two modes is around 0.7 dB and the power in the side modes at 1547 nm is 20 dB less than that of the DFB1 mode at 1548.65 nm. This optical signal is detected by a high speed photodiode (100 GHz bandwidth), and the resulting electrical signal is downmixed to 2.8 GHz with a Virginia Diodes Inc. Sub-harmonic mixer VDI WR08 mixer using a 51.3 GHz LO. The RF signal at the output of the photodiode has an electrical power of –11 dBm (1.25 mA into a 50 Ω load), and a 3 dB spectral width of about 10 MHz.

Data modulation at 1 Gbps is applied to the output SOA (Mod) of the integrated dual wavelength signal source. The optical output is coupled into a lensed fiber followed by three isolators to minimize the fiber reflection, coupling up to 6 dBm of optical power. This optical output is connected to our high speed photodiode (which has a DC responsivity of 0.48 A/W, with a 6 dB reduction at 120 GHz). The output of the photodiode is connected to a 23 dBi F-band (90–140 GHz) horn antenna.

On the receiver end, a 20 dBi horn antenna is connected to the VDI sub-harmonic mixer to down-convert the RF to an IF signal, which is detected with a 3.5 GHz real time scope through a 20 dB gain RF amplifier. The real time scope is set to 10 Gs/s sampling rate, and sequences of 0.1 ms duration are recorded, corresponding to 10^5 bits for 1 Gbps modulation, to allow us to perform BER computation through post-processing

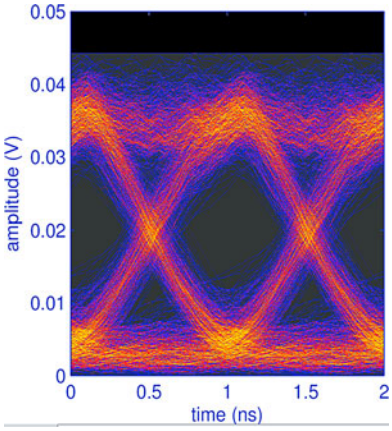

Fig. 15. Eye diagram for 1 Gbps modulation with a modulation current of 7 mA. The PD DC current is 1.7 mA. No error is detected.

by performing a filtered envelope detector function. It is clear from the eye diagram shown in Fig. 15 that a modulation rate of 1 Gbps supports an open, error free signal. Higher data rates were tested, but the performance deteriorated significantly at 2 Gbps. We have found that back reflections at the facets cause a long cavity to form, using the boost SOA as gain section. This limits modulation bandwidth, and indicates that tilting the output waveguides 7° with respect to the chip facets is not sufficient to suppress back reflections, making AR coatings a requirement.

V. Conclusion

We have presented two different photonic integrated circuit approaches to generate carrier waves within the millimeter-wave frequency range. The approach using two monolithically integrated DFB lasers has the main advantage of the frequency tuning range, covering from 5 to 110 GHz in a single device. In addition, a process flow allowing fabrication on the same chip of lasers, optical amplifiers, modulators, and wide-bandwidth UTC photodiodes has been demonstrated. Electrical output powers up to –12 dBm at 95.7 GHz have been achieved. Using a dual DFB source from this fabrication batch, we have achieved wireless data transmission in which the data modulation signal has been directly introduced onto the chip. We have thus demonstrated the potential to integrate a photonic millimeter wave transmitter on a single chip, with an electrical data and bias inputs and an electrical output.

We also report for the first time a new class of dual wavelength sources, based on AWG lasers, which can be integrated within a chip thanks to the use on monolithic MIR reflectors. Although the emission wavelengths are fixed by the channel pass-bands of the AWG, this structure shows very narrow optical mode linewidths (below 200 kHz) without using any phase noise reduction scheme. In addition, thanks to the possibility of adding as many channels as needed in the design stage, it is straightforward to use these devices to generate signals within the THz region.

References

[1] "Cisco visual networking index: Global mobile data traffic forecast update, 2012–2017," Cisco Systems, Inc., San Jose, CA, USA, Feb. 2013.
[2] T. Kleine-Ostmann and T. Nagatsuma, "A review on terahertz communication research," *J. Infrared Milli Terahz Waves*, vol. 32, pp. 143–171, 2011.
[3] H. J. Song and T. Nagatsuma, "Present and future of terahertz communications," *IEEE Trans. Terahertz Sci. Technol.*, vol. 1, no. 1, pp. 256–263, Sep. 2011.
[4] A. Hirata, T. Kosugi, H. Takahashi, J. Takeuchi, H. Togo, M. Yaita, N. Kukutsu, K. Aihara, K. Murata, Y. Sato, T. Nagatsuma, and Y. Kado, "120-GHz-band wireless link technologies for outdoor 10-Gbit/s data transmission," *IEEE Trans. Microw. Theory Techn.*, vol. 60, no. 3, pp. 881–895, Mar. 2012.
[5] I. Kallfass, J. Antes, T. Schneider, F. Kurz, D. Lopez-Diaz, S. Diebold, H. Massler, A. Leuther, and A. Tessmann, "All active mmic-based wireless communication at 220 GHz," *IEEE Trans. Terahertz Sci. Technol.*, vol. 1, no. 2, pp. 477–487, Nov. 2011.
[6] A. Stöhr, S. Babiel, P. J. Cannard, B. Charbonnier, F. Van-Dijk, S. Fedderwitz, D. Moodie, L. Pavlovic, L. Ponnampalam, C. C. Renaud, D. Rogers, V. Rymanov, A. Seeds, A. G. Steffan, A. Umbach, and M. Weiss, "Millimeter-wave photonic components for broadband wireless systems,"*IEEE Trans. Microw. Theory Techn.*, vol. 58, no. 11, pp. 3071–3082, Nov. 2010.
[7] L. A. Johansson and A. J. Seeds, "Generation and transmission of millimeter-wave data-modulated optical signals using an optical injection phase-lock loop," *J. Lightw. Technol.*, vol. 21, no. 2, pp. 511–520, Feb. 2003.
[8] F. Van-Dijk, A. Accard, A. Enard, O. Drisse, D. Make, and F. Lelarge, "Monolithic dual wavelength DFB lasers for narrow linewidth heterodyne beat-note generation," in *Proc. Int. Top. Meeting Microw. Photon.*, Oct. 18–21, 2011, pp. 73–76.
[9] T. Gobel, D. Stanze, R. J. B. Dietz, H. Roehle, M. Schlak, B. Sartorius, and M. Schell, "Next generation continuous wave photomixing THz systems,"in *Proc. 36th Int. Conf. Infrared, Millimeter Terahertz Waves*, Oct. 2–7, 2011, pp. 1–2.
[10] iPHOS project (www.iphos-project.eu) Jun. 2010–Nov. 2013.
[11] M. J. Fice, E. Rouvalis, F. van Dijk, A. Accard, F. Lelarge, C. C. Renaud, G. Carpintero, and A. J. Seeds, "146-GHz millimeter-wave radio-over-fiber photonic wireless transmission system," *Opt. Exp.*, vol. 20, pp. 1769–1774, 2012.
[12] M. Smit, X. Leijtens, E. Bente, J. van der Tol, H. Ambrosius, D. Robbins, M. Wale, N. Grote, and M. Schell, "Generic foundry model for InP-based photonics," *IET Optoelectronics*, vol. 5, no. 5, pp. 187–194, Oct. 2011.
[13] C. R. Doerr, M. Zirngibl, and C. H. Joyner, "Single longitudinal-mode stability via wave mixing in long-cavity semiconductor lasers," *IEEE Photon. Technol. Lett.*, vol. 7, no. 9, pp. 962–964, Sep. 1995.
[14] G. Carpintero, E. Rouvalis, K. Ławniczuk, M. Fice, C. C. Renaud, X. J. M. Leijtens, E. A. J. M. Bente, M. Chitoui, F. Van Dijk, A. J. Seeds, "95 GHz millimeter wave signal generation using an arrayed waveguide grating dual wavelength semiconductor laser," *Opt. Lett.*, vol. 37, pp. 3657–3659, 2012.
[15] E. Rouvalis, M. Chtioui, M. Tran, F. Lelarge, F. van Dijk, M. J. Fice, C. C. Renaud, G. Carpintero, and A. J. Seeds, "High-speed photodiodes for InP-based photonic integrated circuits," *Opt. Exp.*, vol. 20, pp. 9172–9177, 2012.
[16] E. Kleijn, M. K. Smit, and X. J. M. Leijtens, "Multimode interference reflectors: A new class of components for photonic integrated circuits," *J. Lightw. Technol.*, vol. 31, no. 18, pp. 3055–3063, Sep. 15, 2013.
[17] T. Okoshi, K. Kikuchi, and A. Nakayama, "Novel method for high resolution measurement of laser output spectrum," *Electron. Lett.*, vol. 16, pp. 630–631, 1980.
[18] A. Jimenez, R. C. Guzman, L. E. Garcia-Munoz, D. Segovia, and G. Carpintero, "Continuous wave millimeter and terahertz generation using a photonic integrated circuit," in *Proc. 38th Int. Conf. Infrared, Millimeter, Terahertz Waves*, Sep. 1–6, 2013, p. 1.

Authors' biographies not available at the time of publication.